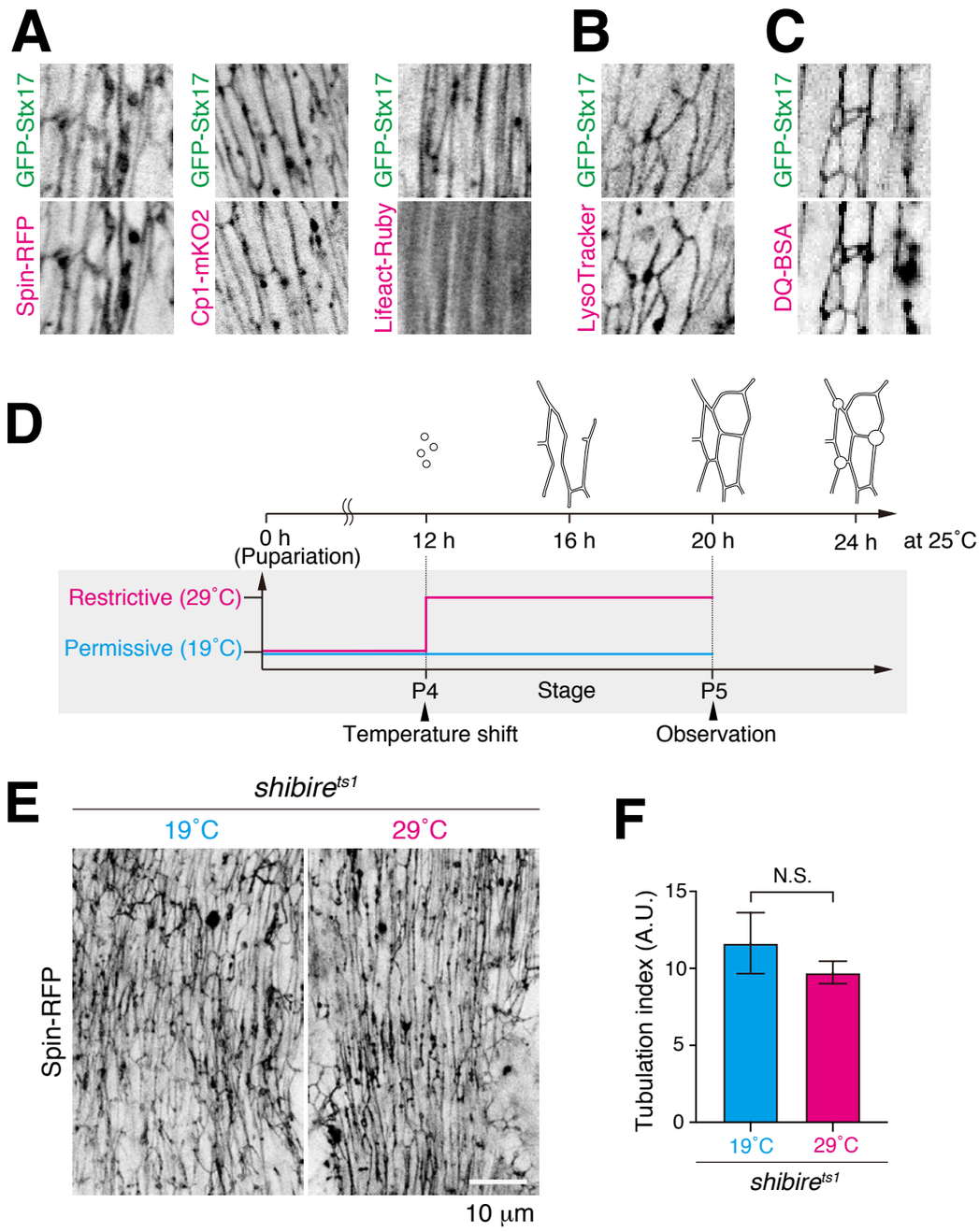

Figure S1

Figure S1 Minimal effect of *shibire* disruption on tAL network formation

(A) Colocalization between GFP–Stx17 and Spin–RFP, Cp1–mKO2, or Lifeact–Ruby in 20 h APF DIOMs. Single channels were shown. (B and C) Live pupae were injected with LysoTracker Red (B) or DQ Red-BSA (C), and DIOMs were imaged through the cuticle at 20 h APF. Single channels were shown. (D) Scheme of an experiment using *shibire* temperature-sensitive mutant (shi^{ts1}). shi^{ts1} mutant was incubated at 19˚C all the time (Permissive) or 29˚C from P4 to P5 stage (Restrictive). (E and F) Spin–RFP-positive tubular network in DIOM at P5 stage (E). Quantification of the Spin–RFP-positive tubules in panel E (F). The average ± SD is shown, n=5. NS, not significant; (Student's *t*-test).

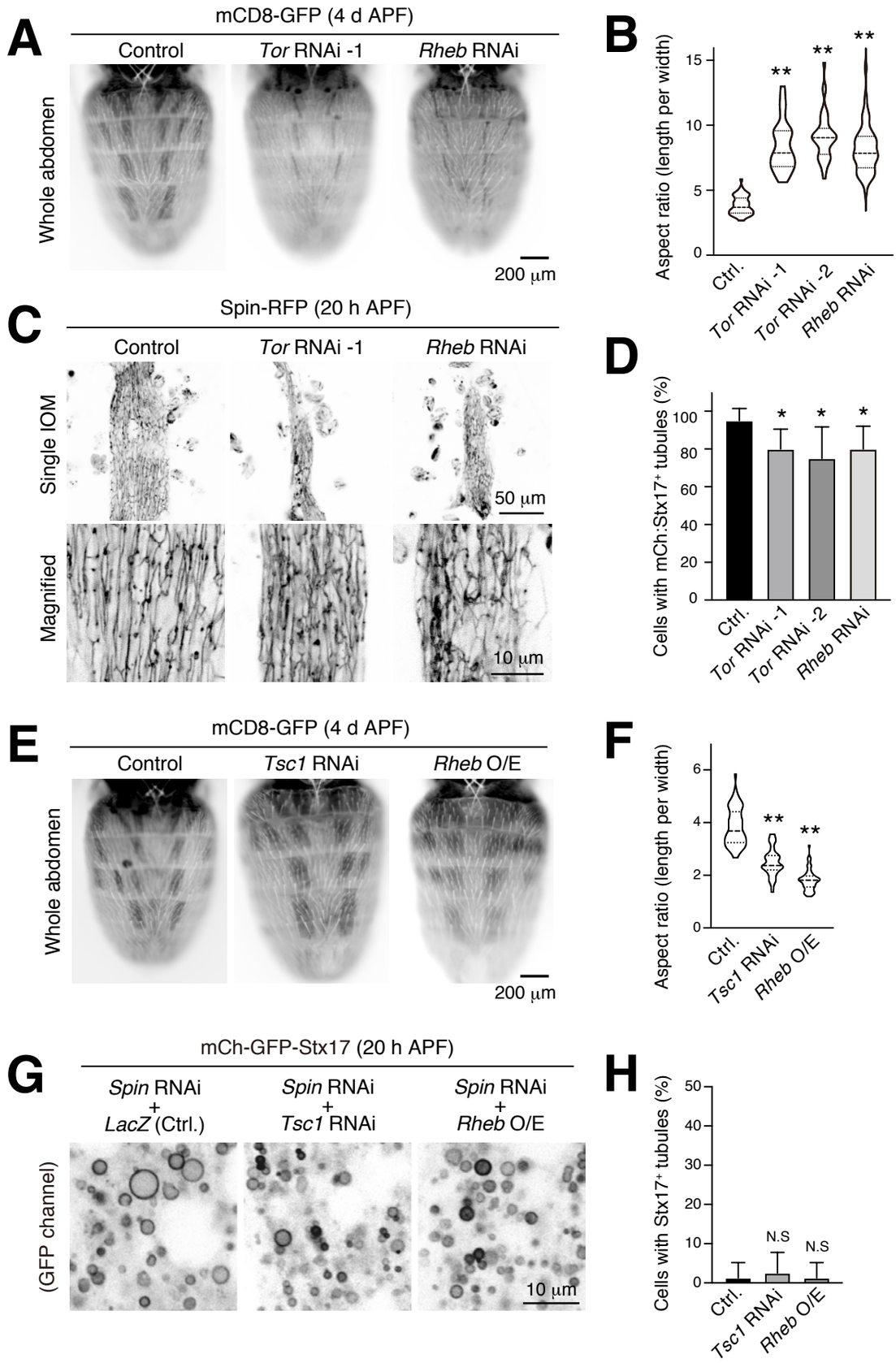

Figure S2

Figure S2 Forced activation or inactivation of mTOR in DIOMs

(A and B) Effect of forced mTOR inactivation on the shape of DIOMs at 4 d APF (A). Violin plot of the aspect ratio of DIOMs, n>40. **, p<0.001 (Dunnett's test) (B). (C and D) Effect of forced mTOR inactivation on the formation of the Spin–RFP-positive tubular structures in 20 h APF DIOMs (C). Mean percent + SD of DIOMs with Spin–RFP-positive tubules, n=10. *, p<0.05 (Dunnett's test) (D). (E and F) Effect of forced mTOR activation on the shape of DIOMs at 4 d APF (E). Violin plot of the aspect ratio of DIOMs, n>50. **, p<0.001 (Dunnett's test) (F). (G and H) Genetic interaction between *Spin* and mTOR regulators. Combination of *Spin* RNAi and *Tsc1* RNAi or *Rheb* overexpression on mCherry–GFP–Stx17-positive structures in 20 h APF DIOMs (G). Mean percent + SD of DIOMs with Stx17-positive tubules, n=10. N.S, not significant (Dunnett's test) (H).

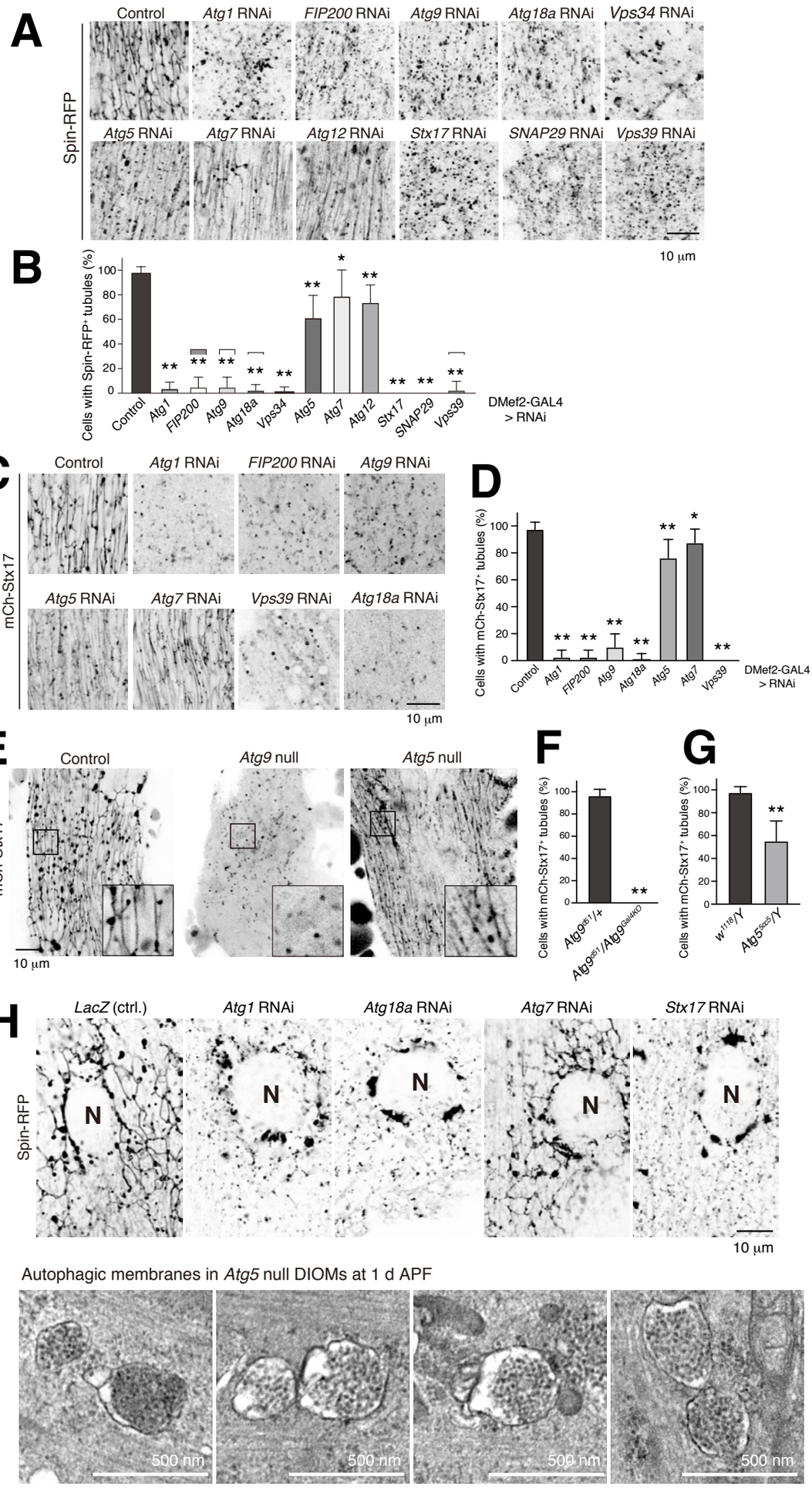

Figure S3

Figure S3 Loss of *ATG* genes on the tubular autolysosome network

(A and B) Effect of RNAi of autophagy-related (*ATG*) genes on Spin–RFP-positive tubular network in 20 h APF DIOMs (A). Mean percent + SD of DIOMs with more than 5 μm Spin–RFP-positive tubules, n=10. *, $p<0.05$; **, $p<0.001$ (Dunnett's test) (B).

(C and D) Effect of RNAi of autophagy-related genes on mCherry–Stx17-positive tubules in 20 h APF DIOMs (C). Mean percent + SD of DIOMs with more than 5 μm mCherry–Stx17-positive tubules, n=10. *, $p<0.05$; **, $p<0.001$ (Dunnett's test) (D). (E-G) mCherry–Stx17 in control, *Atg9* null, or *Atg5* null DIOMs at 20 h APF (E). Mean percent + SD of DIOMs with more than 5 μm mCherry–Stx17-positive tubules in control or *Atg9* null, n=10 (F), control or *Atg5* null, n=10 (G). **$p<0.001$ (Student's *t*-test). (H) Effect of RNAi of autophagy-related genes on Spin–RFP-positive tubules in 3IL body wall muscle. The images are sections close to the sarcolemma. N, nucleus. (I) Typical double-membraned structures in the electron micrograms of *Atg5* null DIOMs at 20 h APF.

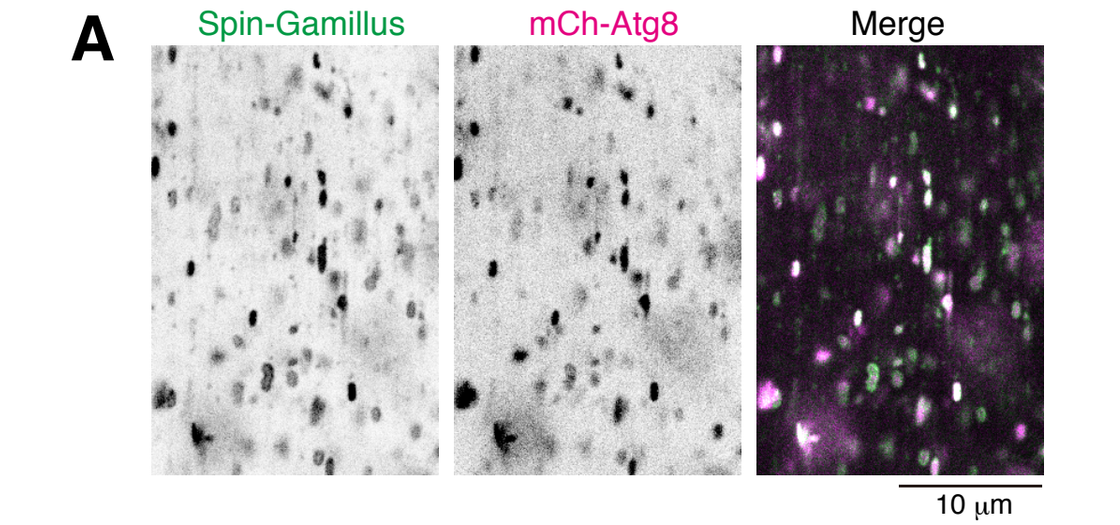

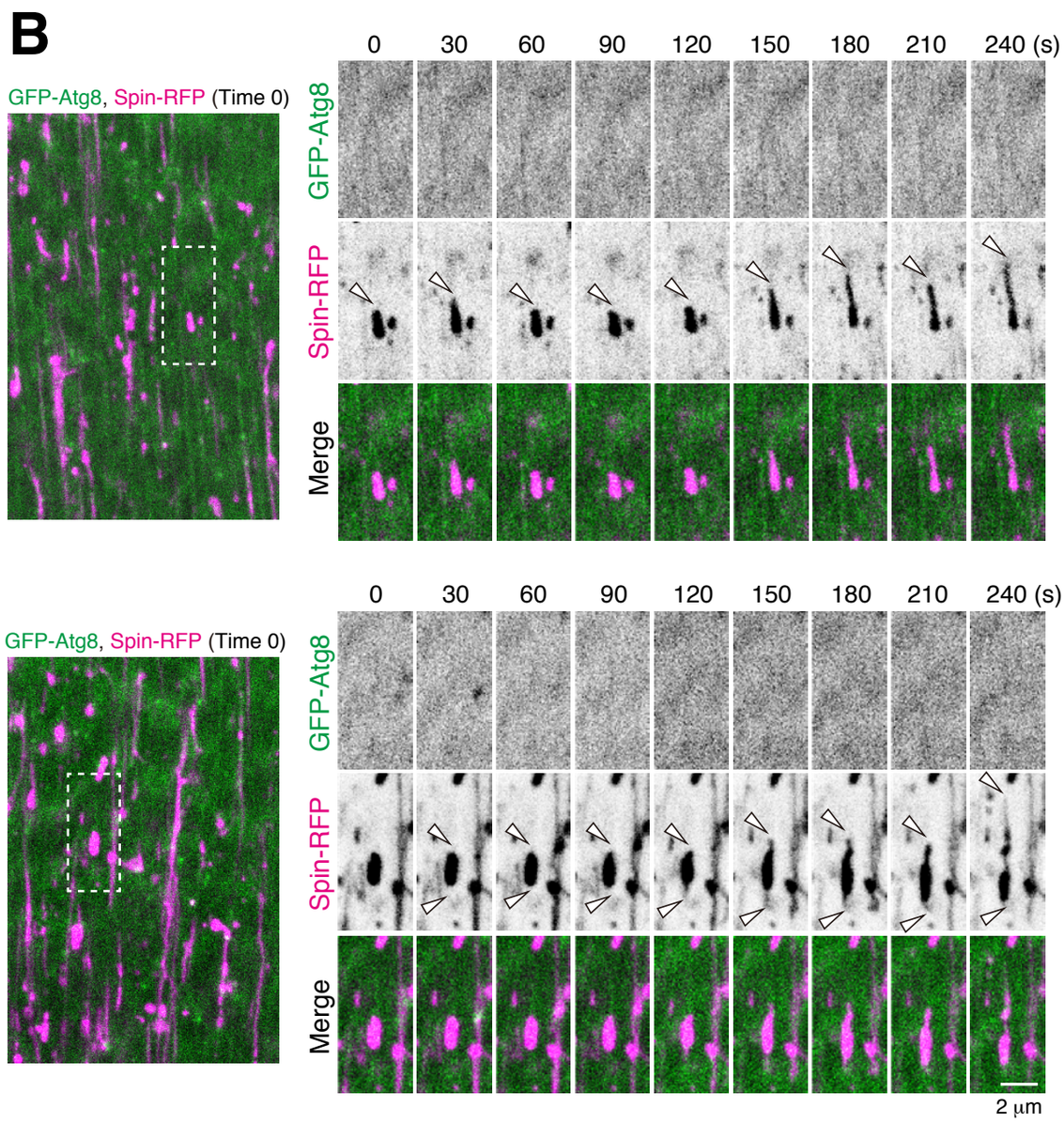

Figure S4

Figure S4 Autophagosome fusion is a prerequisite for the initial tubulation process in the tAL network formation

(A) Colocalization between Spin–Gamillus and mCh–Atg8a in 12 h APF DIOMs. (B) Time-lapse imaging of Spin–RFP and GFP–Atg8a in control DIOMs around 14 h APF. White arrowheads indicate the tips of elongating tubules.

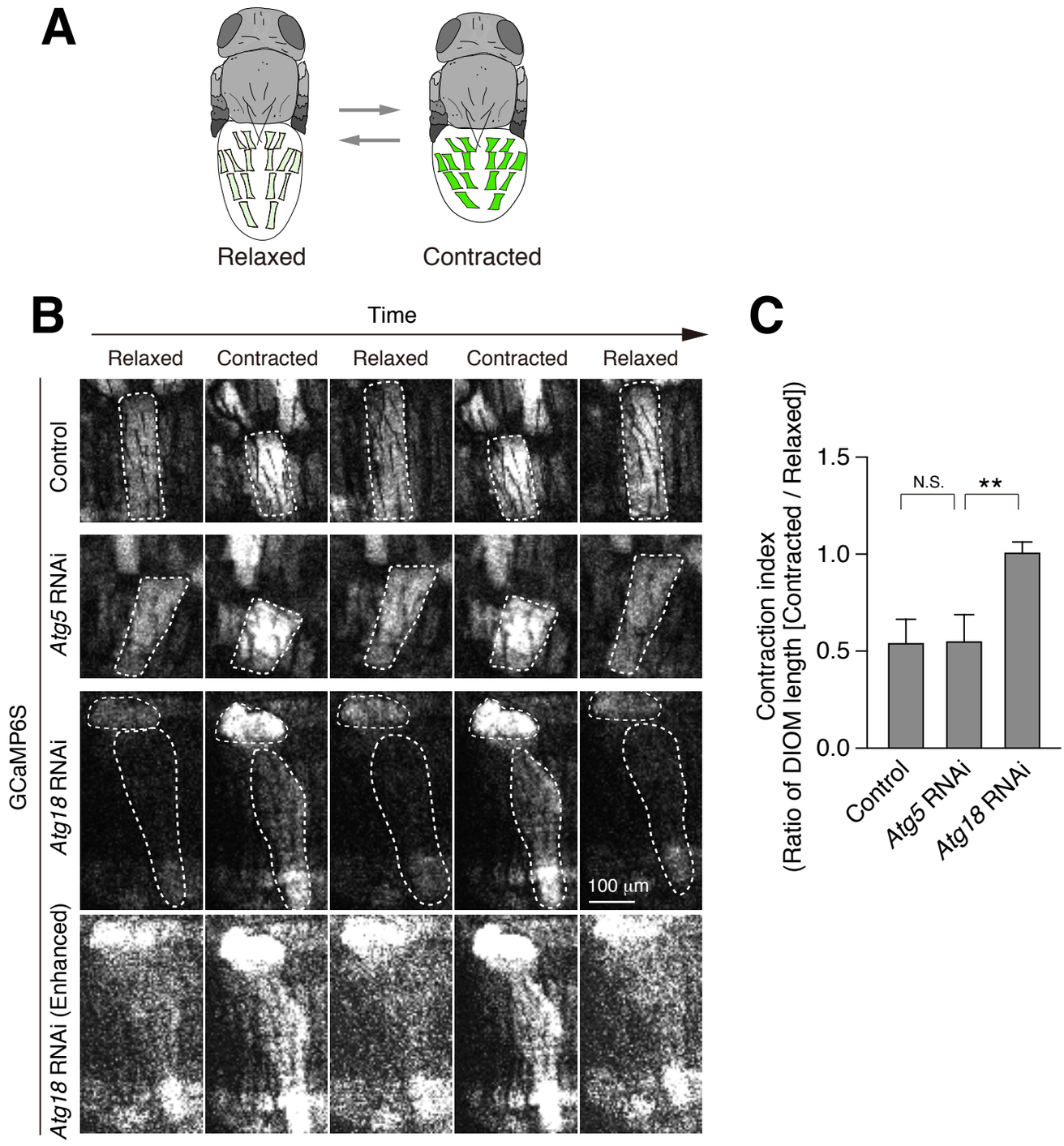

Figure S5

Figure S5 Contractile function of *ATG*-RNAi DIOMs upon the elevation of Ca^{2+} levels

(A) Schematic model of DIOM contraction in 4 d APF fly. GCaMP6S signal becomes brighter upon the elevation of cytosolic Ca^{2+} levels in DIOMs. (B) Time-lapse imaging of GCaMP6S in 4 d APF DIOMs of control, *Atg5* RNAi, or *Atg18a* RNAi. Two contraction cycles were shown for each. (C) Mean percent + SD of DIOM contraction index. The index is defined as the length of contracted DIOM divided by that of relaxed DIOMs. Four contractions of single DIOM were analyzed and averaged. N=5. N.S, not significant; **, $p<0.001$ (Dunnett's test).

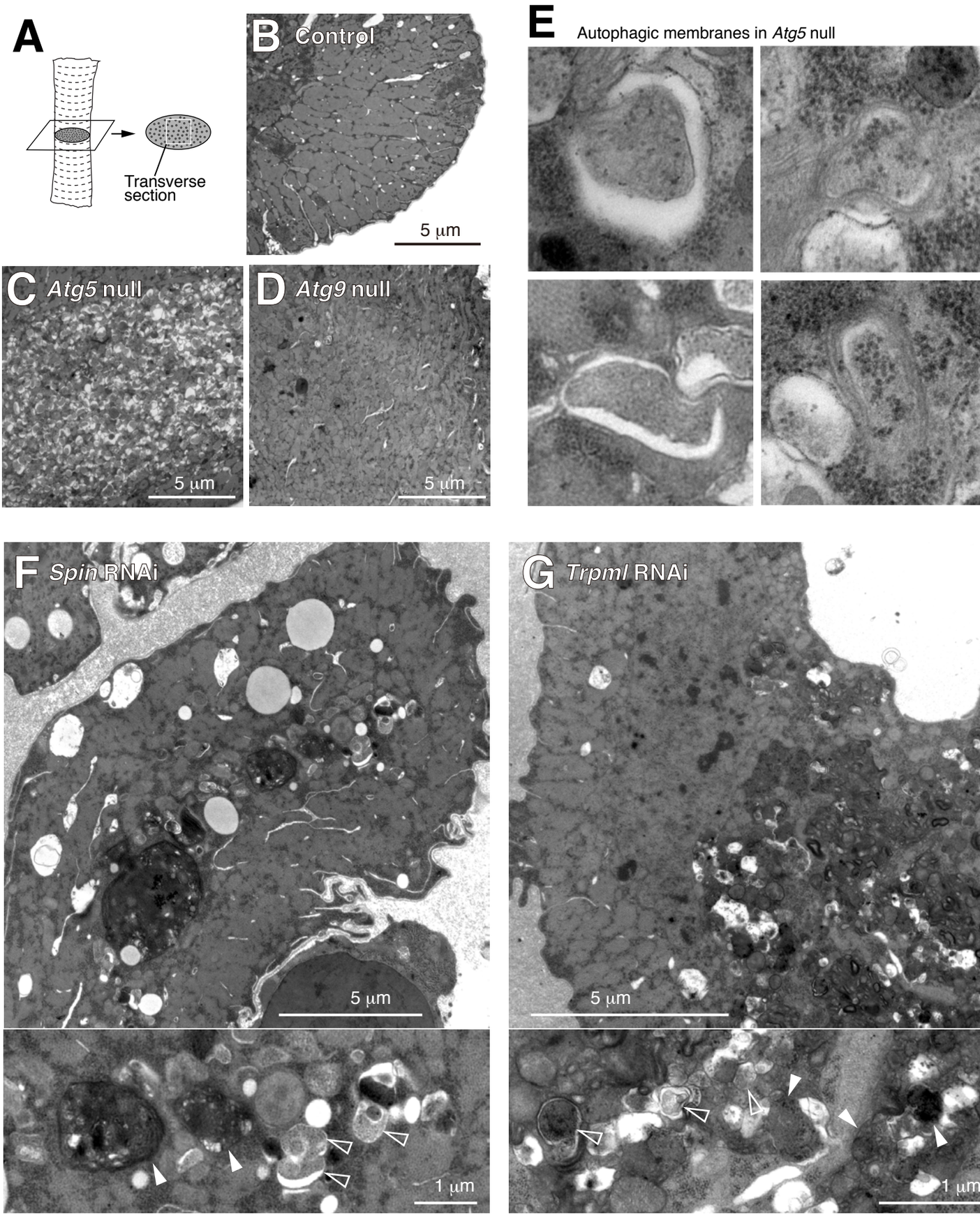

Figure S6

Figure S6 Ultrastructure of 4 d APF DIOMs of *Atg5* null, *Atg9* null, *Spin* RNAi, or *Trpml* RNAi

(A) Schematic of a DIOM TEM transverse section. (B-D) TEM images of 4 d APF DIOM transverse-section of control (B), *Atg5* null (C), or *Atg9* null (D). (E) Typical examples of autophagic structures in *Atg5* null DIOMs at 4 d APF. (F and G) TEM images of 4 d APF DIOM transverse-section of *Spin* RNAi (F) or *Trpml* RNAi (G). Autolysosome, white arrowhead; autophagosome, colorless arrowhead.

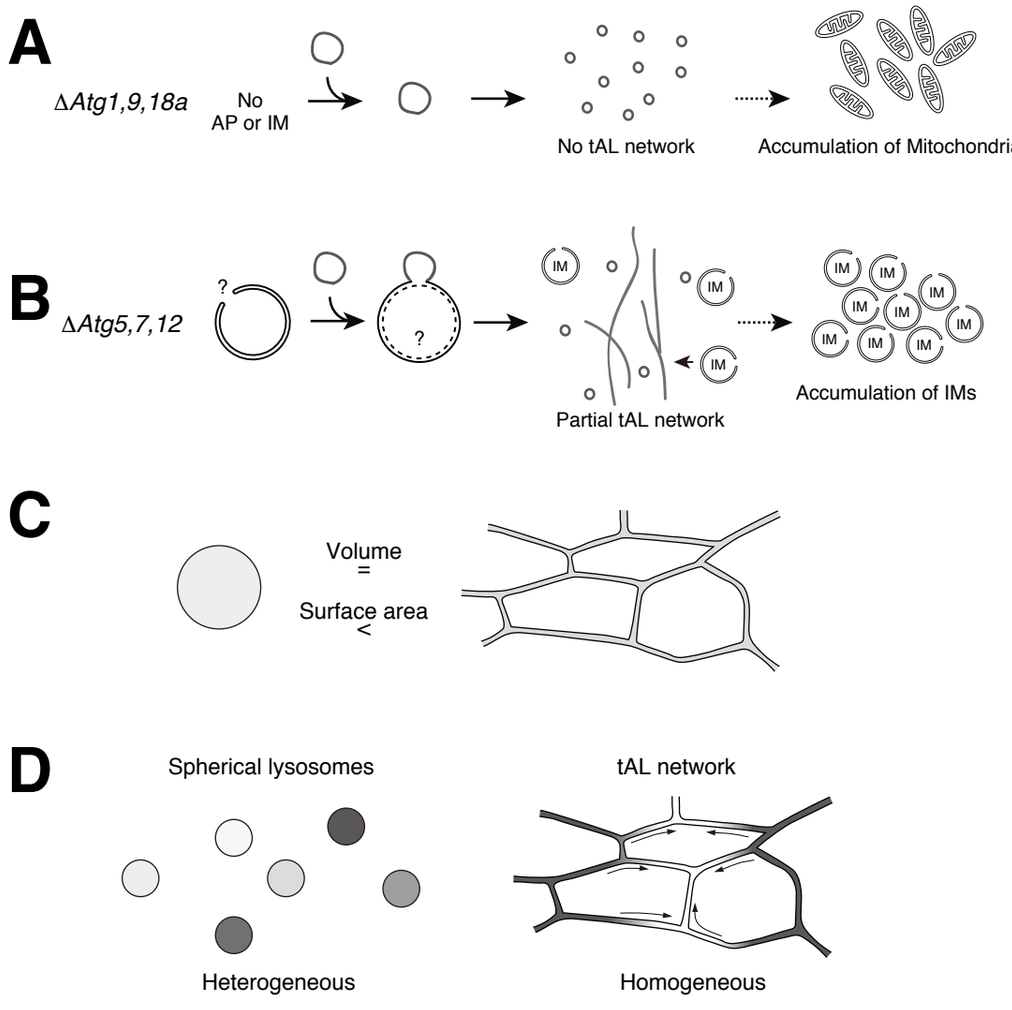

Figure S7

Figure S7 Possible model of the tAL network formation and its significance

(A) No autophagic membrane in loss of *Atg1*, *9*, or *18a*, which results in no tAL network.

(B) Fusion of late isolation membranes with lysosomes leads to partially defective tAL network in loss of *Atg5*, *7*, or *12*. (C) A ratio of surface area per volume of a ranging between 50 to 70-nm-diameter tube and 500-nm-diameter spherical vesicle. The tube has ~5 times higher score than that of the vesicle. (D) The tAL network is homogeneous over a wide range compared to a number of spherical, discontinuous lysosomes.

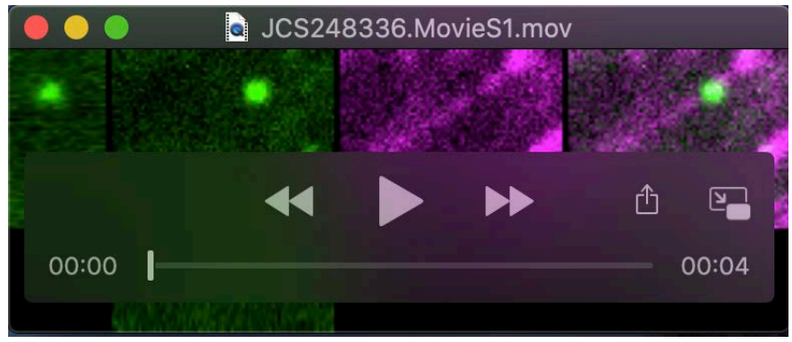

Movie 1 Time-lapse imaging of Spin:RFP and GFP:Atg8a in 20 h APF DIOMs

The DIOM expressing both Spin:RFP and GFP:Atg8a was imaged every 60 s for 30 min on an inverted microscope with a spinning-disc confocal scanner unit and a CMOS camera. Z-stacked images were shown.

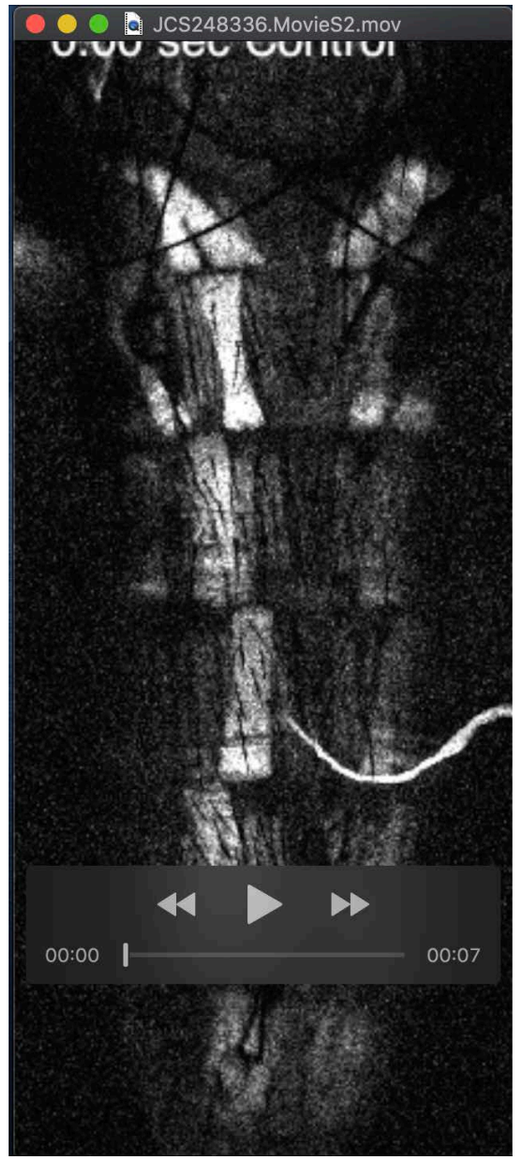

Movie 2 Time-lapse imaging of contraction of control DIOMs

Four days APF DIOMs expressing GCaMP6S and LacZ (control) was imaged every 570 ms for 85 s (150 frames) by confocal laser scanning microscope.

Movie 3 Time-lapse imaging of contraction of *Atg5* RNAi DIOMs

Four days APF DIOMs expressing GCaMP6S and IR-*Atg5* (*Atg5* RNAi) was imaged every 570 ms for 85 s (150 frames) by confocal laser scanning microscope.

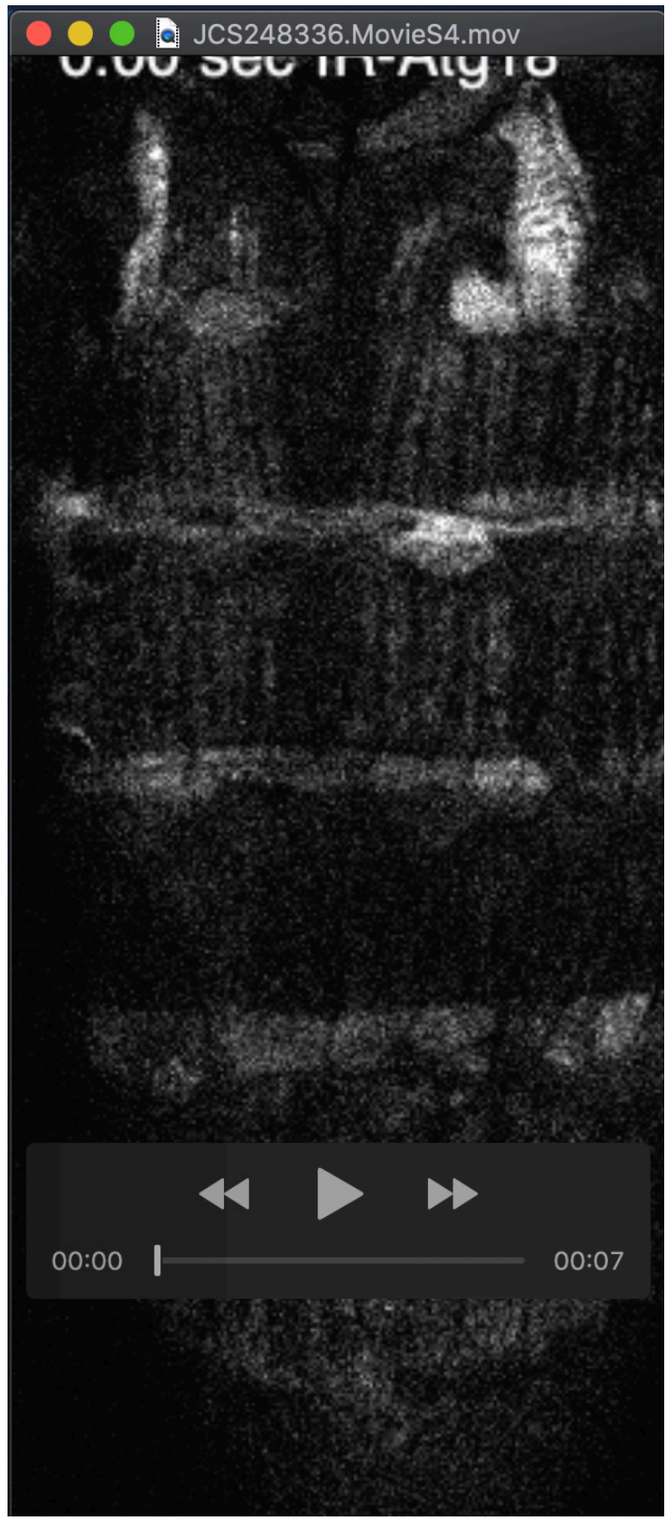

Movie 4 Time-lapse imaging of contraction of *Atg18* RNAi DIOMs

Four days APF DIOMs expressing GCaMP6S and IR-*Atg18* (*Atg18* RNAi) was imaged every 570 ms for 85 s (150 frames) by confocal laser scanning microscope.

Table S1. Detailed *Drosophila* genotypes shown in figures

	Panel #	Genotype	Stage	Temp (˚C)	Microscopy
Figure 1	1B	*UAS-mCD8:GFP/+; DMef2-GAL4/+*	3IL to 4 d APF	25˚C	FV1000D
	1C	*DMef2-GAL4/UAS-GFP:Stx17*	3IL to 4 d APF	25˚C	FV1000D
	1D	*DMef2-GAL4/UAS-GFP:Stx17*	12 to 20 h APF	25˚C	FV1000D
Figure 2	2A	*UAS-mCh:GFP:Atg8a/+; DMef2-GAL4/+*	3IL to 4 APF	25˚C	FV1000D
	2B	*UAS-mCh:Atg8a/+; DMef2-GAL4, UAS-GFP:Stx17/+*	20 h APF	25˚C	FV1000D
	2C	*UAS-Spin:myc:RFP/+; DMef2-GAL4, UAS-GFP:Stx17/+*	20 h APF	25˚C	FV1000D
		DMef2-GAL4, UAS-GFP:Stx17/UAS-Cp1:mKO2	20 h APF	25˚C	FV1000D
		UAS-Lifeact:Ruby/+; DMef2-GAL4, UAS-GFP:Stx17/+	20 h APF	25˚C	FV1000D
	2D	*DMef2-GAL4/UAS-GFP:Stx17* (Injection of Lysotracker Red)	20 h APF	25˚C	FV3000
	2E	*DMef2-GAL4/UAS-GFP:Stx17* (Injection of DQ-BSA)	20 h APF	25˚C	FV3000
	2F	*UAS-GFP:Atg8a/UAS-Spin:myc:RFP; DMef2-GAL4/+*	20 h APF	25˚C	Dragonfly
	2H and I	*UAS-LacZ/+; DMef2-GAL4, UAS-GFP:Stx17/+*	20 h APF	25˚C	FV1000D
		UAS-IR-Spin$^{NIG8428R-4}$/+; DMef2-GAL4, UAS-GFP:Stx17/+	20 h APF	25˚C	FV1000D
		UAS-IR-Trpml^{HMS02818}/+; DMef2-GAL4, UAS-GFP:Stx17/+	20 h APF	25˚C	FV1000D
		DMef2-GAL4, UAS-GFP:Stx17/UAS-IR-Vha68-3$^{NIG5075R-1}$	20 h APF	25˚C	FV1000D
Figure 3	3A	*w/Y; UAS-Spin:RFP/+; DMef2-GAL4, UAS-Dcr2/+*	20 h APF	25˚C	FV1000D
	3B	*Atg5^{5cc5}/Y; UAS-Spin:myc:RFP/+; DMef2-GAL4, UAS-Dcr2/+*	20 h APF	25˚C	FV1000D
	3C	*w/Y; Atg9^{d51}, UAS-Spin:myc:RFP/Atg9^{Gal4KO}; DMef2-GAL4, UAS-Dcr2/+*	20 h APF	25˚C	FV1000D
	3D	*w/Y; Atg9^{d51}, UAS-Spin:myc:RFP/+; DMef2-GAL4, UAS-Dcr2/+*	20 h APF	25˚C	-
		w/Y; Atg9^{d51}, UAS-Spin:myc:RFP/Atg9^{Gal4KO}; DMef2-GAL4, UAS-Dcr2/+	20 h APF	25˚C	-
	3E	*UAS-Spin:myc:RFP/+; DMef2-GAL4, Stx17^{LL}/Stx17^{Df_Exel18098}*	20 h APF	25˚C	FV1000D
	3F	*UAS-Spin:myc:RFP/+; DMef2-GAL4, Stx17^{LL}/+*	20 h APF	25˚C	-
		UAS-Spin:myc:RFP/+; DMef2-GAL4, Stx17^{LL}/Stx17^{Df_Exel18098}	20 h APF	25˚C	-
	3G	*Atg5^{5cc5}/Y; UAS-Spin:myc:RFP/+; DMef2-GAL4, UAS-IR-Stx17^{JF01937}/+*	20 h APF	25˚C	FV1000D
	3H	*w/Y; UAS-Spin:myc:RFP/+; DMef2-GAL4, UAS-Dcr2/+*	20 h APF	25˚C	-
		Atg5^{5cc5}/Y; UAS-Spin:myc:RFP/+; DMef2-GAL4, UAS-Dcr2/+	20 h APF	25˚C	-
		Atg5^{5cc5}/Y; UAS-Spin:myc:RFP/+; DMef2-GAL4, UAS-IR-Stx17^{JF01937}/+	20 h APF	25˚C	-
	3I and J	*UAS-IR-Spin, UAS-mCh:GFP:Stx17/UAS-LacZ; DMef2-GAL4, UAS-Dcr2, tub-GAL80^{ts}*	20 h APF	25˚C	FV1000D
		UAS-IR-Spin, UAS-mCh:GFP:Stx17/UAS-IR-Atg18a^{v105366}; DMef2-GAL4, UAS-Dcr2, tub-GAL80^{ts}/+	20 h APF	25˚C	FV1000D
		UAS-IR-Spin, UAS-mCh:GFP:Stx17/UAS-IR-Vps39^{HMS02438}; DMef2-GAL4, UAS-Dcr2, tub-GAL80^{ts}/+	20 h APF	25˚C	FV1000D
Figure 4	4A	*w; +/+; +/+*	20 h APF	25˚C	H-7100
	4B	*w; Atg9^{d51}/Atg9^{Gal4KO}; +/+*	20 h APF	25˚C	H-7100
	4C	*w; +/+; FIP200^{3FG}/FIP200^{4G7}*	20 h APF	25˚C	H-7100
	4D	*Atg5^{5cc5}/Y; +/+; +/+*	20 h APF	25˚C	H-7100
	4E and F	*w; +/+; +/+*	20 h APF	25˚C	H-7100
	4G	*UAS-IR-Spin$^{NIG8428R-4}$/+; DMef2-GAL4, UAS-Dcr2/+*	20 h APF	25˚C	H-7100
	4H	*UAS-IR-Trpml^{HMS02818}/+; DMef2-GAL4, UAS-Dcr2/+*	20 h APF	25˚C	H-7100
Figure 5	A-C	*UAS-Spin:myc:RFP/UAS-LacZ; DMef2-GAL4, UAS-Dcr2/+*	14 h APF	25˚C	FV3000
	D	*UAS-Spin:myc:RFP/+; DMef2-GAL4, UAS-Dcr2/UAS-IR-Stx17^{JF01937}*	14 h APF	25˚C	FV3000
Figure 6	6A and B	*UAS-mCD8:GFP/UAS-LacZ; DMef2-GAL4, UAS-Dcr2/+*	4 d APF	25˚C	SZX16
		UAS-mCD8:GFP/+; DMef2-GAL4, UAS-Dcr2/UAS-IR-Atg5$^{NIG1643R-2}$	4 d APF	25˚C	SZX16
		UAS-mCD8:GFP/+; DMef2-GAL4, UAS-Dcr2/UAS-IR-Atg12^{HMS01153}	4 d APF	25˚C	SZX16
		UAS-mCD8:GFP/+; DMef2-GAL4, UAS-Dcr2/UAS-IR-FIP200^{HMS01611}	4 d APF	25˚C	SZX16
		UAS-mCD8:GFP/+; DMef2-GAL4, UAS-Dcr2/UAS-IR-Atg9^{HMS01246}	4 d APF	25˚C	SZX16
		UAS-mCD8:GFP/UAS-IR-Atg18a^{v105366}; DMef2-GAL4, UAS-Dcr2/+	4 d APF	25˚C	SZX16
	6C and D	*w/Y; +/+; +/+*	4 d APF	25˚C	FV1000D
		Atg5^{5cc5}/Y; +/+; +/+	4 d APF	25˚C	FV1000D
		w/Y; Atg9^{d51}/Atg9^{Gal4KO}; +/+	4 d APF	25˚C	FV1000D
	6E	*UAS-Dcr2/UAS-LacZ; DMef2-GAL4, Sph-YFP:Mito/+*	4 d APF	25˚C	FV1000D
		UAS-Dcr2/+; DMef2-GAL4, Sph-YFP:Mito/UAS-IR-Atg5$^{NIG1643R-2}$	4 d APF	25˚C	FV1000D
		UAS-Dcr2/+; DMef2-GAL4, Sph-YFP:Mito/UAS-IR-Atg9^{HMS01246}	4 d APF	25˚C	FV1000D
	6F	*UAS-Dcr2/UAS-LacZ; DMef2-GAL4, UAS-GFP:Stx17/+*	4 d APF	25˚C	FV1000D
		UAS-Dcr2/+; DMef2-GAL4, UAS-GFP:Stx17/UAS-IR-Atg5$^{NIG1643R-2}$	4 d APF	25˚C	FV1000D
		UAS-Dcr2/+; DMef2-GAL4, UAS-GFP:Stx17/UAS-IR-Atg9^{HMS01246}	4 d APF	25˚C	FV1000D
	6G	*w/Y; +/+; +/+*	4 d APF	25˚C	H-7100
	6H	*Atg5^{5cc5}/Y; +/+; +/+*	4 d APF	25˚C	H-7100
	6I	*w/Y; Atg9^{d51}/Atg9^{Gal4KO}; +/+*	4 d APF	25˚C	H-7100
Figure 7	7A	*DMef2-GAL4, UAS-Cp1:mKO2/UAS-GFP:Stx17*	24 h APF	25˚C	FV3000
	7C	*UAS-Dcr2/UAS-LacZ; DMef2-GAL4, UAS-Cp1:mKO2, UAS-GFP:Stx17/+*	24 h APF	25˚C	FV3000
	7D	*UAS-Spin$^{NIG8428R-4}$/UAS-Dcr2; DMef2-GAL4, UAS-Cp1-mKO2, UAS-GFP-Stx17/+*	24 h APF	25˚C	FV3000
Figure 8	8A and B	*DMef2-GAL4/UAS-GFP:Stx17* (Injection of Lysotracker Red)	24 h APF	25˚C	FV3000
	8C and D	*DMef2-GAL4/UAS-GFP:Stx17* (Injection of DQ-BSA)	24 h APF	25˚C	FV3000
	8E-H	*w; UAS-GFP/UAS-LacZ; DMef2-GAL4, UAS-Dcr2/+*	24 h APF	25˚C	FV3000
		w; UAS-GFP/UAS-IR-Atg18a^{v105366}; DMef2-GAL4, UAS-Dcr2/+	24 h APF	25˚C	FV3000

Figure S1	S1A	*UAS-Spin:myc:RFP/+; DMef2-GAL4, UAS-GFP:Stx17/+*	20 h APF	25˚C	FV1000D
		DMef2-GAL4, UAS-GFP:Stx17/UAS-Cp1:mKO2	20 h APF	25˚C	FV1000D
		UAS-Lifeact:Ruby/+; DMef2-GAL4, UAS-GFP:Stx17/+	20 h APF	25˚C	FV1000D
	S1B	*DMef2-GAL4/UAS-GFP:Stx17* (Injection of Lysotracker Red)	20 h APF	25˚C	FV3000
	S1C	*DMef2-GAL4/UAS-GFP:Stx17* (Injection of DQ-BSA)	20 h APF	25˚C	FV3000
	S1E and F	*shi[1]/y; +/UAS-Spin-RFP; +/DMef2-GAL4, UAS-Dcr2*	P5	19˚C	FV3000
		shi[1]/y; +/UAS-Spin-RFP; +/DMef2-GAL4, UAS-Dcr2	P5	19 > 29˚C	FV3000
Figure S2	S2A and B	*UAS-mCD8:GFP/UAS-LacZ; DMef2-GAL4, UAS-Dcr2/+*	4 d APF	25˚C	SZX16
		UAS-mCD8:GFP/+; DMef2-GAL4, UAS-Dcr2/UAS-IR-TOR^{GL00156} (*Tor* RNAi -1)	4 d APF	25˚C	SZX16
		UAS-mCD8:GFP/+; DMef2-GAL4, UAS-Dcr2/UAS-IR-TOR^{HMS01114} (*Tor* RNAi -2)	4 d APF	25˚C	SZX16
		UAS-mCD8:GFP/+; DMef2-GAL4, UAS-Dcr2/UAS-IR-Rheb^{HMS00923}	4 d APF	25˚C	SZX16
	S2C and D	*UAS-Spin:myc:RFP/UAS-LacZ; DMef2-GAL4, UAS-Dcr2/+*	20 h APF	25˚C	FV1000D
		UAS-Spin:myc:RFP/+; DMef2-GAL4, UAS-Dcr2/UAS-IR-TOR^{GL00156} (*Tor* RNAi -1)	20 h APF	25˚C	FV1000D
		UAS-Spin:myc:RFP/+; DMef2-GAL4, UAS-Dcr2/UAS-IR-TOR^{HMS01114} (*Tor* RNAi -2)	4 d APF	25˚C	FV3000
		UAS-Spin:myc:RFP/+; DMef2-GAL4, UAS-Dcr2/UAS-IR-Rheb^{HMS00923}	20 h APF	25˚C	FV1000D
	S2E and F	*UAS-mCD8:GFP/UAS-LacZ; DMef2-GAL4, UAS-Dcr2/+*	4 d APF	25˚C	SZX16
		UAS-mCD8:GFP/+; DMef2-GAL4, UAS-Dcr2/UAS-IR-Tsc1^{GL00012}	4 d APF	25˚C	SZX16
		UAS-mCD8:GFP/+; DMef2-GAL4, UAS-Dcr2/UAS-Rheb.Pa	4 d APF	25˚C	SZX16
	S2G and H	*UAS-IR-Spin, UAS-mCh:GFP:Stx17/UAS-LacZ; DMef2-GAL4, UAS-Dcr2, tub-GAL80^{ts}*	20 h APF	25˚C	FV1000D
		UAS-IR-Spin, UAS-mCh:GFP:Stx17/+; DMef2-GAL4, UAS-Dcr2, tub-GAL80^{ts}/UAS-IR-TSC1^{GL00012}	20 h APF	25˚C	FV1000D
		UAS-IR-Spin, UAS-mCh:GFP:Stx17/+; DMef2-GAL4, UAS-Dcr2, tub-GAL80^{ts}/UAS-Rheb.Pa	20 h APF	25˚C	FV1000D
Figure S3	S3A and B	*UAS-Spin:myc:RFP/UAS-LacZ; DMef2-GAL4, UAS-Dcr2/+*	20 h APF	25˚C	FV1000D
		UAS-Spin:myc:RFP/UAS-IR-Atg1; DMef2-GAL4, UAS-Dcr2/+	20 h APF	25˚C	FV1000D
		UAS-Spin:myc:RFP/+; DMef2-GAL4, UAS-Dcr2/UAS-IR-FIP200^{HMS01611}	20 h APF	25˚C	FV1000D
		UAS-Spin:myc:RFP/+; DMef2-GAL4, UAS-Dcr2/UAS-IR-Atg9^{HMS01246}	20 h APF	25˚C	FV1000D
		UAS-Spin:myc:RFP/UAS-IR-Atg18a^{v105366}; DMef2-GAL4, UAS-Dcr2/+	20 h APF	25˚C	FV1000D
		UAS-Spin:myc:RFP/+; DMef2-GAL4, UAS-Dcr2/UAS-IR-Vps34$^{NIG5373R-2}$	20 h APF	25˚C	FV1000D
		UAS-Spin:myc:RFP/+; DMef2-GAL4, UAS-Dcr2/UAS-IR-Atg5$^{NIG1643R-2}$	20 h APF	25˚C	FV1000D
		UAS-Spin:myc:RFP/+; DMef2-GAL4, UAS-Dcr2/UAS-IR-Atg7$^{NIG5489R-2}$	20 h APF	25˚C	FV1000D
		UAS-Spin:myc:RFP/+; DMef2-GAL4, UAS-Dcr2/UAS-IR-Atg12^{HMS01153}	20 h APF	25˚C	FV1000D
		UAS-Spin:myc:RFP/+; DMef2-GAL4, UAS-Dcr2/UAS-IR-Stx17^{JF01937}	20 h APF	25˚C	FV1000D
		UAS-Spin:myc:RFP/+; DMef2-GAL4, UAS-Dcr2/UAS-IR-SNAP29^{JF01883}	20 h APF	25˚C	FV1000D
		UAS-Spin:myc:RFP/UAS-IR-Vps39^{HMS02438}; DMef2-GAL4, UAS-Dcr2/+	20 h APF	25˚C	FV1000D
	S3C and D	*UAS-Dcr2/UAS-LacZ; DMef2-GAL4, UAS-mCh:Stx17/+*	20 h APF	25˚C	FV1000D
		UAS-Dcr2/UAS-IR-Atg1; DMef2-GAL4, UAS-mCh:Stx17/+	20 h APF	25˚C	FV1000D
		UAS-Dcr2/+; DMef2-GAL4, UAS-mCh:Stx17/UAS-IR-FIP200^{HMS01611}	20 h APF	25˚C	FV1000D
		UAS-Dcr2/+; DMef2-GAL4, UAS-mCh:Stx17/UAS-IR-Atg9^{HMS01246}	20 h APF	25˚C	FV1000D
		UAS-Dcr2/UAS-IR-Atg18a^{v105366}; DMef2-GAL4, UAS-mCh:Stx17/+	20 h APF	25˚C	FV1000D
		UAS-Dcr2/+; DMef2-GAL4, UAS-mCh:Stx17/UAS-IR-Atg5$^{NIG1643R-2}$	20 h APF	25˚C	FV1000D
		UAS-Dcr2/+; DMef2-GAL4, UAS-mCh:Stx17/UAS-IR-Atg7$^{NIG5489R-2}$	20 h APF	25˚C	FV1000D
		UAS-Dcr2/UAS-IR-Vps39^{HMS02438}; DMef2-GAL4, UAS-mCh:Stx17/+	20 h APF	25˚C	FV1000D
	S3E	*Atg9^{d51}/+; DMef2-GAL4, UAS-mCh:Stx17/+*	20 h APF	25˚C	FV1000D
		Atg9^{d51}/Atg9^{Gal4KO}; DMef2-GAL4, UAS-mCh:Stx17/+	20 h APF	25˚C	FV1000D
		Atg5^{5cc5}/Y; +/+; DMef2-GAL4, UAS-mCh:Stx17/+	20 h APF	25˚C	FV1000D
	S3F	*Atg9^{d51}/+; DMef2-GAL4, UAS-mCh:Stx17/+*	20 h APF	25˚C	-
		Atg9^{d51}/Atg9^{Gal4KO}; DMef2-GAL4, UAS-mCh:Stx17/+	20 h APF	25˚C	-
	S3G	*w/Y; +/+; DMef2-GAL4, UAS-mCh:Stx17/+*	20 h APF	25˚C	-
		Atg5^{5cc5}/Y; +/+; DMef2-GAL4, UAS-mCh:Stx17/+	20 h APF	25˚C	-
	S3H	*UAS-Spin:myc:RFP/UAS-LacZ; DMef2-GAL4, UAS-Dcr2/+*	3IL	25˚C	FV1000D
		UAS-Spin:myc:RFP/UAS-IR-Atg1; DMef2-GAL4, UAS-Dcr2/+	3IL	25˚C	FV1000D
		UAS-Spin:myc:RFP/UAS-IR-Atg18a^{v105366}; DMef2-GAL4, UAS-Dcr2/+	3IL	25˚C	FV1000D
		UAS-Spin:myc:RFP/UAS-IR-Atg7^{HMS01358}; DMef2-GAL4, UAS-Dcr2/+	3IL	25˚C	FV1000D
		UAS-Spin:myc:RFP/+; DMef2-GAL4, UAS-Dcr2/UAS-IR-Stx17^{JF01937}	3IL	25˚C	FV1000D
	S3I	*Atg5^{5cc5}/Y; +/+; +/+*	20 h APF	25˚C	H-7100
Figure S4	S4A	*UAS-spin:Gamillus/UAS-mCh:Atg8a; Dmef2-GAL4, UAS-Dcr2/+*	12 h APF	25˚C	FV3000
	S4B	*UAS-GFP:Atg8a/UAS-Spin:myc:RFP; DMef2-GAL4/+*	14 h APF	25˚C	FV3000
Figure S5	S5B and C	*UAS-Dcr2/UAS-LacZ; DMef2-GAL4, UAS-GCaMP6S/+*	4 d APF	25˚C	FV3000
		UAS-Dcr2/+; DMef2-GAL4, UAS-GCaMP6S/UAS-IR-Atg5$^{NIG1643R-2}$	4 d APF	25˚C	FV3000
		UAS-Dcr2/UAS-IR-Atg18a^{v105366}; DMef2-GAL4, UAS-GCaMP6S/+	4 d APF	25˚C	FV3000
Figure S6	S6B	*w/Y; +/+; +/+*	4 d APF	25˚C	H-7100
	S6C	*Atg5^{5cc5}/Y; +/+; +/+*	4 d APF	25˚C	H-7100
	S6D	*w/Y; Atg9^{d51}/Atg9^{Gal4KO}; +/+*	4 d APF	25˚C	H-7100
	S6E	*Atg5^{5cc5}/Y; +/+; +/+*	4 d APF	25˚C	H-7100
	S6F	*UAS-IR-Spin$^{NIG8428R-4}$/+; DMef2-GAL4, UAS-Dcr2/+*	4 d APF	25˚C	H-7100
	S6G	*UAS-IR-Trpml^{HMS02818}/+; DMef2-GAL4, UAS-Dcr2/+*	4 d APF	25˚C	H-7100